



An aprotic lithium/polyiodide semi-liquid battery with an ionic shield



Y.X. Ren^{a,1}, M. Liu^{a,1}, T.S. Zhao^{a,*}, L. Zeng^b, M.C. Wu^a

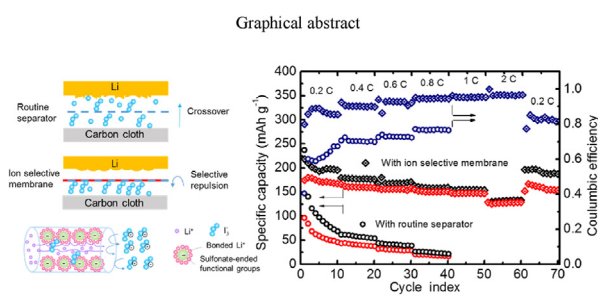
^a Department of Mechanical and Aerospace Engineering, The Hong Kong University of Science and Technology, Clear Water Bay, Kowloon, Hong Kong Special Administrative Region

^b HKUST Jockey Club Institute for Advanced Study, The Hong Kong University of Science and Technology, Clear Water Bay, Kowloon, Hong Kong SAR, China

HIGHLIGHTS

- An ion selective aprotic Li/polyiodide semi-liquid battery was demonstrated.
- The polyiodide shuttles can be suppressed by the electrostatic repulsion.
- A high energy density of 170.5 Wh L⁻¹ was attained with 1.5 M LiI₃ catholyte.
- Stable cycling was achieved with a capacity retention over 84% for 100 cycles.

GRAPHICAL ABSTRACT



ARTICLE INFO

Article history:

Received 7 October 2016
 Received in revised form
 9 December 2016
 Accepted 12 December 2016
 Available online 16 December 2016

Keywords:

Lithium/polyiodide battery
 Shuttle effect
 Ion selective membrane
 Electrostatic repulsion

ABSTRACT

In this paper, we report a high-energy-density lithium/polyiodide (Li/PI) semi-liquid battery with soluble polyiodide in ether-based solvents as the catholyte. The challenge of shuttle effect is addressed by adopting a hybrid membrane coated with negatively charged sulfonate-ended perfluoroalkyl polymer, which allows for inhibition of polyiodide shuttles due to the electrostatic repulsion. The assembled Li/PI battery demonstrates a superior volumetric energy density (170.5 Wh L⁻¹), a stable cycling performance (>100 cycles, averaged decay < 0.16% at 0.2 C), a high energy efficiency (>84%, 100 cycles at 2 C), and a high coulombic efficiency (>95%, 100 cycles at 2 C). These high performances achieved suggest that the aprotic Li/polyiodide battery with a compact architecture has the potential for various energy storage applications.

© 2016 Elsevier B.V. All rights reserved.

1. Introduction

The development of high-energy-density and efficient scaled-up electrical energy storage (EES) systems becomes a focal point for distributed electric grids, especially with the ever-increasing deployment of wind and solar powers, which suffers from their intermittent and fluctuating nature [1–5]. Among the existing EES systems, lithium based batteries promise superior energy density and excellent reversibility, thus the efforts to innovate the lithium

based batteries for scaled-up energy storage have never ceased [6–12]. Beyond using solid-state cathode host for Li-ions, exploring strategies to dissolve the active material in the solution phase catholyte have drawn increasing attentions, which are attributed to their underlying superiorities of (i) faster mass transport in the liquid phase catholyte, (ii) more facile electron transfer across a liquid/solid interface and (iii) the flexibility of designing the scaled-up systems with decoupled energy storage and power output [13–16].

In light of these merits, Lu and Goodenough proposed the prototype of a hybrid semi-liquid battery using an alkaline metal (for example, lithium metal) and an aqueous cathode containing redox-

* Corresponding author.

E-mail address: metzhao@ust.hk (T.S. Zhao).

¹ These authors contributed equally to this work.

active species (for example, ferricyanide), separated by a glass ceramic membrane [17,18]. Also employing the aqueous cathode configuration, Zhao et al. conceived a series of development for halogen-based cathodes, demonstrating remarkable battery performances, especially in terms of the energy density and cycling stability [19–23]. However, the critical demand for a crack-free glass ceramic membrane renders it challenging to scale up the lithium/aqueous configuration. Due to the fragile and resistive nature of the solid state electrolyte, it is still on its pathway to meet the requirement of developing a sufficiently robust Li/aqueous system.

The application of non-aqueous catholytes possibly mitigates the above inconvenience. Towards high-energy-density storage and stable performance, redox-active species in non-aqueous systems are under exploration. One direction is the organic redox compounds (e.g., ferrocene-based, TEMPO-based), which is still an ongoing effort [14,15]. The other concerns for the efficient utilization of the inorganic redox couples including iron, halogen and chalcogen-based redox couples [20]. For such batteries, the solubility and the stability of the redox couples to pair with the lithium anode become target issues to be considered. Recently, emerging efforts have been paid in developing non-aqueous Li-S flow batteries. The Li-S battery chemistry enables a relatively stable passivation layer on the Li anode, which possibly realizes a membrane-free design, however, due to the inferior solubility of short-chain Li_2S_n ($n = 1, 2, 4$), the recently developed Li-S flow battery with a volumetric energy density of 30 Wh L^{-1} didn't exhibit superior advantages over the vanadium redox flow battery (VRFB) systems (25 Wh L^{-1}) [13,24]. Towards a higher energy density, one of the promising alternatives is the I_3^-/I^- redox couple, which is capable of simultaneously compromising among the demands of fast reaction kinetics, non-toxicity nature and high solubility [22,23,25]. During the discharge-charge process, the cathodic reaction occurs as $\text{I}_3^- + 2\text{e}^- \leftrightarrow 3\text{I}^-$. By using a 3 M LiI catholyte for example, the volumetric capacity can reach as high as 53.5 A h L^{-1} , resulting in a volumetric energy density around 150 Wh L^{-1} , which far more exceeds the conventional redox flow batteries [26].

With the high solubility of polyiodide in the aprotic solvents ($\sim 9 \text{ M I}^-$ in DOL/DME), self-discharge as well as infinite charging is a serious problem facing such aprotic Li/PI batteries. On the Li anode surface, polyiodide anions can be chemically or electrochemically reduced to iodide anions ($2\text{Li} + \text{I}_3^- \rightarrow 2\text{Li}^+ + 3\text{I}^-$ or $\text{I}_3^- + 2\text{e}^- \rightarrow 3\text{I}^-$), lowering the battery's coulombic efficiency. For those reported Li/iodine batteries, approaches for immobilizing the iodine into a host material (e.g. carbon) were exploited [27,28]. However, binding between the carbon materials and polyiodide species was found to be intrinsically weak [28]. Unlike polysulfides, it is challenging to identify suitable materials to chemically anchor the polyiodide [29]. On the other hand, lithium nitrate as an electrolyte additive has been introduced into the Li/iodine batteries, which contributes to generate a chemically stable passivation layer onto the Li anode to retard the shuttle effect [28,30]. Unfortunately, the multidimensional Li growth during the cycling process usually leads to the collapse of the passivation layer [31–33]. Due to above reasons, to our knowledge, the aprotic semi-liquid Li/polyiodide battery that directly utilizes the liquid catholyte, has not been reported until today. In addition to above strategies, we note that for cation exchange membranes (CEMs) in fuel cells and chlor-alkali industry, anions can be excluded from CEMs by an electrostatic repulsion from the negatively charged functional groups on the membrane, which is a phenomenon referred to as the Donnan exclusion [34–37]. In this regard, when an ion selective membrane is incorporated, possibly the Li/polyiodide battery performance can be efficiently improved by localizing those polyiodide anions within

the cathode side by the electrostatic repulsion effect.

Motivated by this issue, we designed and fabricated a proof-of-concept rechargeable lithium/polyiodide (Li/PI) semi-liquid battery with a Nafion-functionalized composite membrane for the ion selective Li/PI configuration. After a lithiation process, the penetrated Nafion in the porous membrane enabled the transport of Li^+ ions while mitigating the diffusion of polyiodide anions to the anode side due to the electrostatic repulsion between the negatively charged perfluorinated functional groups and polyiodide anions. Consequently, the cycling stability of Li/PI batteries with such a Nafion-functionalized composite membrane was dramatically improved, with a cycle decay rate below 0.16% for over 100 cycles at 0.2 C.

2. Experimental

2.1. Material preparation

The polyiodide (LiI_3) solution was prepared by dissolving a desired amount of stoichiometric I_2 and LiI in 1,3-dioxolane (DOL)/1,2-dimethoxyethane (DME) solution (1:1 in volume) with the addition of 1 M LiTFSI and 1 wt% LiNO_3 additive ($\sim 0.15 \text{ M}$). For the typical preparation of 1 M LiI_3 solution, 1.27 g of elemental I_2 and 0.67 g of LiI were added to 5 mL of DOL/DME (1:1) based electrolyte. The obtained suspension was stirred for 1 h to yield a red-brown LiI_3 solution.

Polypropylene membranes (Celgard 2500, porosity 55%, 1.40 mg cm^{-2}) were coated with the Nafion solution (1 wt% in dimethylformamide (DMF) solution) and dried on a hotplate at 80°C afterward. The Nafion amounts were varied from 0.8, 1.2 and 1.6 mg cm^{-2} . To lithiate the as-prepared membranes, the membranes were soaked in the blank electrolyte comprising 1.0 M LiTFSI and 0.15 M LiNO_3 in the DME/DOL (1:1, v/v) solvent for a week [38]. The Celgard separator coated with the lithiated Nafion, which was denoted as the Nafion-functionalized composite membrane, was then used for the battery assembly without any further treatment.

2.2. Cell assembly and test

One piece of lithium (16 mm diameter) was placed onto the bottom of the copper cell body, a layer of Celgard separator or Nafion-functionalized composite membrane (18 mm diameter) was placed onto the lithium foil, followed by the placement of a piece of carbon cloth (12 mm diameter, hydrophilic). As previously reported in the literature, the overhang method, namely using an electrode with a smaller size than the Li anode, can decrease the dendrite growth [32]. Herein, a circular carbon cloth with a smaller diameter (12 mm) was exploited and 25 μL as-prepared catholyte containing LiI_3 with various concentrations (0.33 M, 1 M and 1.5 M) were injected into batteries without further addition of blank electrolyte. The theoretical capacities (I_2/I^-) for three groups of batteries were determined as 0.67, 2.0 and 3.0 mAh respectively. To avoid the unexpected iodine precipitation, the batteries were cycled in a voltage range of 2–3.4 V.

The electrochemical measurements were determined with a potentiostat (Princeton Applied Research, PARSTAT M2273). Electrochemical impedance spectroscopy (EIS) measurement using a frequency range from 100 kHz to 1 Hz with a wave amplitude of 5 mV was applied to the assembled Li/PI batteries after charge. Besides, the cyclic voltammetry (CV) of the assembled Li/PI batteries was tested at a scanning rate of 0.5 mV s^{-1} with the carbon cloth electrode as the working electrode and lithium coil as both reference and counter electrodes.

The visible permeability test to examine the properties of the membranes was carried out in an H-type glass cell. The assembly of

transparent battery was conducted in a glove box to exclude the influence of moisture and oxygen. Routine Celgard 2500 and Nafion-functionalized composite membranes were inserted in the glass cell respectively. Carbon cloth was set in the cathode chamber with the addition of 15 mL 25 mM LiI solution with a theoretical capacity of 10.0 mAh ($\text{LiI} \rightarrow \text{I}_2$), while lithium foil was set in the anode chamber with the addition of 15 mL blank electrolyte. During the test, the visible cell was charged at 1.0 mA cm^{-2} to generate the polyiodide solution and the transport behavior of polyiodide across the membrane was recorded.

2.3. Material characterization

The charged anodes after cycling were washed by pure DME and then dried before SEM observation. A field emission scanning electron microscope (FESEM, JEOL 6700) was used to determine the morphology of the charged anodes with an acceleration voltage of 5 kV. Fourier transform infrared spectroscopy (FTIR) measurements were recorded using Vertex 70 Hyperion 1000 (Bruker) with the assistance of attenuated total reflectance (ATR) accessories. The absorption spectra were recorded from 1800 cm^{-1} to 400 cm^{-1} with a resolution of 4 cm^{-1} .

3. Results and discussion

3.1. Battery configuration and material characterization

As mentioned, the battery configuration of a Li/PI battery consists of a carbon cloth cathode, a metallic lithium anode, and a separator, all of which are immersed in the ether-based electrolyte. In most cases, the separator is a porous membrane without functional groups (e.g. polypropylene (PP), polyethylene (PE), glass fibers), which has pores in submicron dimension and serves solely as an electronic insulator, allowing polyiodide and iodide anions to freely diffuse through the membranes. As the polyiodide anions can react with metallic lithium under room temperature to generate iodide anions, the lithium anode might be considerably degraded during the cycling process. To address this issue, we explore the idea of CEMs, in which the functional groups are negatively charged. To provide the proof-of-the-concept, Nafion as a typical CEM is exploited, and the negatively charged perfluorinated functional groups repulse the polyiodide anions as illustrated in Fig. 1a and b.

Though promising, the commercial Nafion membrane shows a swelling behavior in the organic ether based solvent, leading to a lower mechanical strength and a considerable deformation when compressed [39]. Thus, instead of using a commercial Nafion membrane, we impregnated the Nafion into the pores of the robust

Celgard separator for three folds of benefits: (i) there is minor volume change when soaking in organic solvent; (ii) a lower Nafion loading; (iii) a higher ionic conductivity. As shown in Fig. 2a, it is found that an optimal Nafion loading was achieved at 1.2 mg cm^{-2} for the Nafion-functionalized composite membrane in terms of the battery's discharge capacity. The coulombic efficiency increases at a higher Nafion loading, however the enlarged ionic transportation resistance lowers the active material utilization. That is why the commercial Nafion membrane, even the thinnest Nafion 211 with a Nafion loading of 5 mg cm^{-2} , might not be suitable for use in this case. This message can be further confirmed in the EIS analysis as shown in Fig. S1, where the high-frequency intercept is attributed to the battery's ohmic resistance and the diameter of the semi-circle is attributed to the interfacial and charge transfer resistances of the liquid cathode [8,28]. As shown in Fig. 2b, the battery with a Nafion loading of 1.2 mg cm^{-2} exhibits an ohmic resistance of 19.9Ω , in comparison, for the battery with a routine separator, the ohmic resistance is 7.1Ω . As Nafion coated on the separator surface will be in close contact with the carbon cloth cathode, interfacial resistance can be increased as well, which can be attributed to the enlarged interfacial and charge transfer resistances with an increase in Nafion loading.

Fig. 2c shows the ATR-FTIR results of the Nafion membranes with and without the lithiation process. A concerted shifts observed for the peaks at 1710 cm^{-1} to 1640 cm^{-1} when the counter protons are replaced by the Li^+ ions, which is consistent with the lithiation characteristics in the previous relevant studies [34,35,38,40]. A prelithiation process should be more desirable for improving the battery's performance especially at a higher current density as can be found in Fig. S2. Fig. 2(d–f) compare the SEM morphologies of the lithiated Nafion membrane and the commercial Celgard separator (PP/PE). The routine Celgard separator shows a porous structure with pore dimensions in the submicron scale, which unavoidably allows the migration of the dissolved lithium polyiodide/iodide species between the cathode and the anode. As shown in Fig. 2e, most of the submicron pores have been filled after the infiltrated Nafion loading reaches 0.8 mg cm^{-2} , but it is still not sufficient to cover the entire surface of the separator. When the loading is further increased to 1.2 mg cm^{-2} , a compact film is observed to cover the surface, demonstrating a dense and uniform morphology. However, there will be very slight morphology change when the loading is further increased to 1.6 mg cm^{-2} , despite the increase in thickness as can be speculated, which can be confirmed by the cross sectional view of the as-prepared membranes in Fig. S3. Combining electrochemical performance and morphology characterization, it is reasoned that an optimal Nafion loading exists to form a compact thin film to cover onto the porous separator's surface.

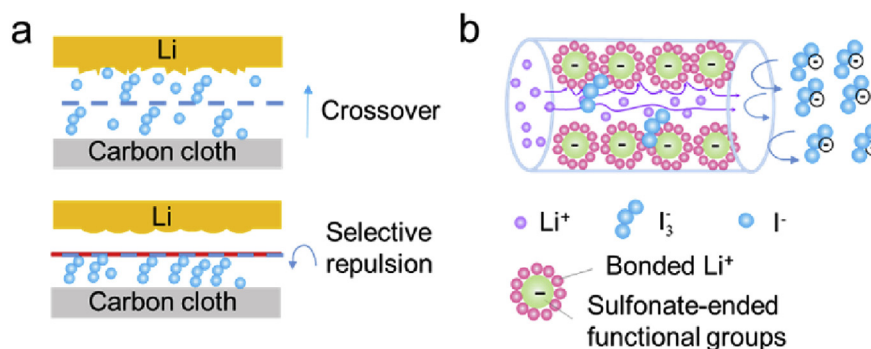


Fig. 1. (a) The schematic illustration of the Li/PI batteries without and with an ion selective membrane. (b) Enlarged schematic for the selective repulsion of polyiodide anions with the use of ion selective membrane (Nafion-functionalized composite membrane).

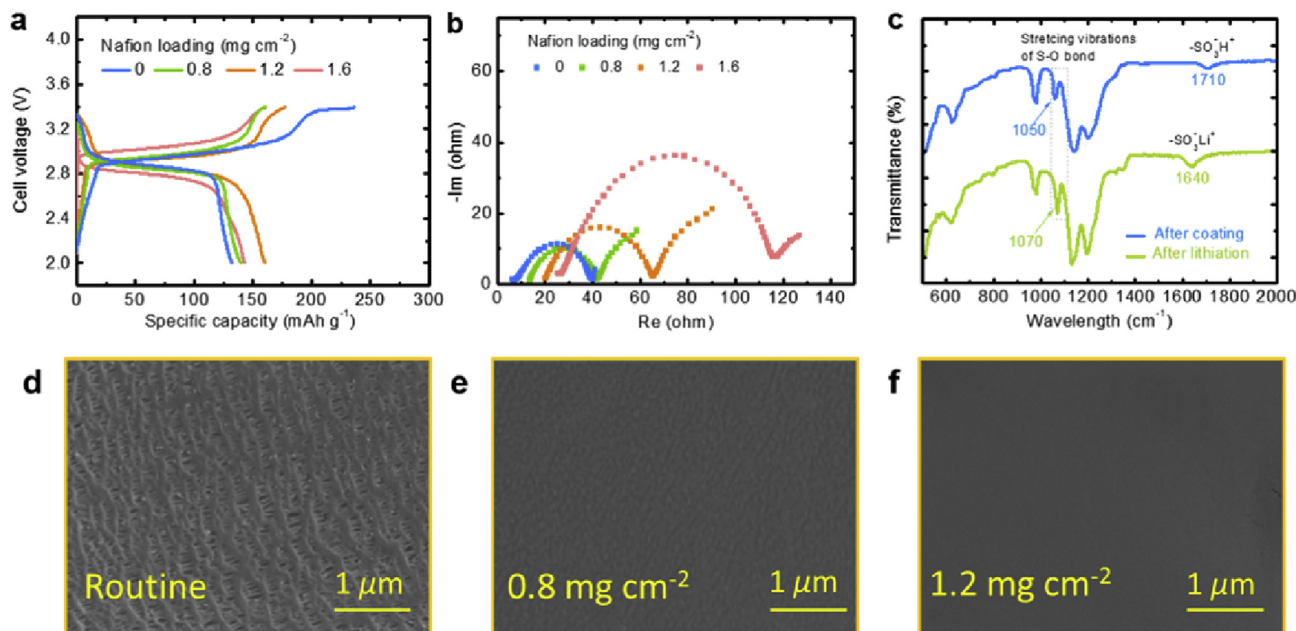


Fig. 2. (a) Charge-discharge curves of Li/PI batteries at 0.6 C using Nafion-functionalized composite membranes with different Nafion loadings (25 μL 0.33 M LiI_3 catholyte was added as the active material). The C rate is calculated based on the specific capacity of elemental iodine (211 mAh g^{-1}). (b) EIS (electrochemical impedance spectroscopy) results of the assembled batteries with different Nafion loadings; (c) FTIR spectra of Nafion-functionalized composite membranes without and with the lithiation process; (d–f) the top view of the routine separator and Nafion-functionalized composite membranes.

In addition to the Nafion loading on the membrane, we herein discuss the effect of catholyte concentration. Because the increase of catholyte concentration renders a higher concentration gradient for the polyiodide crossover, to identify whether the introduction of a Nafion-functionalized composite membrane can sustain in the concentrated catholyte, the performance was tested at 0.33, 1 and 1.5 M LiI_3 . It is found that at a relatively low catholyte concentration, the volumetric capacity can be prolonged, achieving a value slightly exceeding the theoretical capacity of I_3^-/I^- redox couple (e.g. 17.9 Ah L^{-1} for 0.33 M LiI_3 catholyte). It can be seen from the cyclic voltammetry profile in Fig. S4 that there exist two separated anodic peaks representing transformation of I^-/I_3^- (2.78–3.35 V) and I_3^-/I_2 (3.35–3.60 V), respectively. Also, from the galvanostatic curve at the window voltage of 2–3.6 V (Fig. S5), two voltage plateaus can be observed, where the higher voltage plateau represents the redox reaction of I_3^-/I_2 and the lower voltage plateau mostly represents the redox reaction of I^-/I_3^- in consistency with the CV result. Interestingly, it is found that the lower voltage plateau is longer than the two times of the higher voltage plateau, indicating that the redox reaction of I_3^-/I_2 occurs at the lower voltage plateau as well. Based on these result, at a cut-off charge voltage of 3.4 V, I_3^- can be partially oxidized into I_2 and contributes a portion of the discharge capacity. It is worthwhile noting that the solubility of elemental iodine is intrinsically low ($0.60 \pm 0.05 \text{ M I}_2$, 298 K). Hence, a narrow voltage window is desirable if the battery is intended to be operated in a cathode-flow mode with a higher iodide concentration.

When the batteries are cycled at the same rate (1 C), a higher catholyte concentration leads to a higher superficial current. In this regard, the lower catholyte utilization ratio at a higher catholyte concentration can be attributed to the concentration polarization. Herein, at a catholyte concentration of 1.5 M LiI_3 , a catholyte volumetric energy density of 170.5 Wh L^{-1} (60.5 Ah L^{-1}) was achieved. With the increase of catholyte concentration, the overall polyiodide crossover amount becomes larger and the side reactions ($2\text{Li} + \text{I}_3^- \rightarrow 2\text{Li}^+ + 3\text{I}^-$ or $\text{I}_3^- + 2\text{e}^- \rightarrow 3\text{I}^-$) on the Li anode will be

promoted, that is why a slight decrease in coulombic efficiency was found at a higher catholyte concentration (Fig. 3b). Even so, reasonably high energy efficiency (>80%) could be still achieved and the discharge capacities of the as-prepared batteries were well maintained over 10 cycles as shown in Fig. S6 with minor decay. The achieved catholyte volumetric energy density is almost 5 times higher than the all vanadium redox flow batteries do [41]. Also, it should be noted that this value is comparable to the highest reported volumetric energy density for Zn- I_2 flow batteries with an iodide concentration of 10 M [32]. In the next section, the rate and long-term cycling performance of the batteries will be further investigated, for a compromise between the catholyte utilization ratio (specific capacity) and the energy density, an intermediate concentrated catholyte (1 M LiI_3) will be adopted.

3.2. Electrochemical performance

In this section, we further demonstrate the rate and cycling performances of the as-prepared batteries. As presented in Fig. 4a, batteries with the routine separator and Nafion-functionalized composite membrane were operated from 0.2 to 2 C. With a routine separator, the Li anode is exposed to the corrosive electrolyte containing polyiodide and the battery suffers from rapid capacity decay as well as a very low coulombic efficiency ($\sim 40\%$ for the initial cycle at 0.2 C), as can be seen from the first several cycles in Fig. 4b. In sharp contrast, under the introduction of a Nafion-functionalized composite membrane, the resultant battery demonstrated dramatically improved stability as well as excellent capacity retention. The representative charge/discharge profiles at the 5th cycle at different rates are displayed in Fig. 4c. The discharge capacity only decreases for $\sim 20\%$, from 0.2 C to 2 C, implying the fast kinetics of I_3^-/I^- redox couple. Moreover, with an increase of discharge rate, it is found that the coulombic efficiency dramatically increases, indicating that when the discharge time is shortened, the overall crossover amount can be efficiently diminished [42]. This is why Fig. 4a and c show that the coulombic efficiency

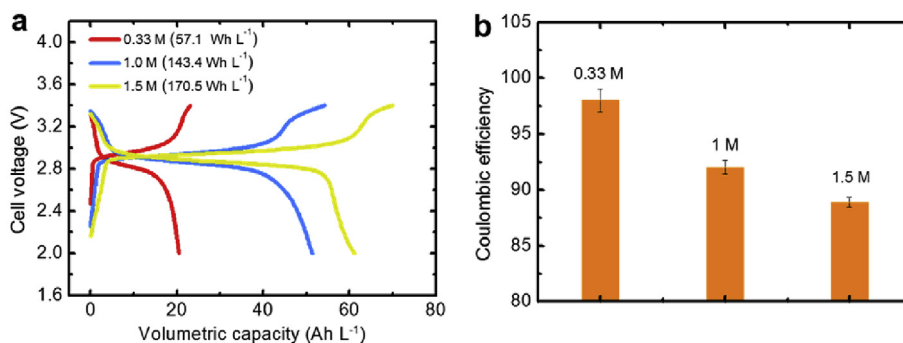


Fig. 3. (a) Charge-discharge curves at different catholyte concentrations (0.33, 1 and 1.5 M LiI₃) at 1 C for the Li/PI batteries with the Nafion-functionalized composite membrane (Nafion loading 1.2 mg cm⁻²); (b) the corresponding effect of catholyte concentration on coulombic efficiency. The volumetric capacity is calculated based on the volume of catholyte volume (25 μL).

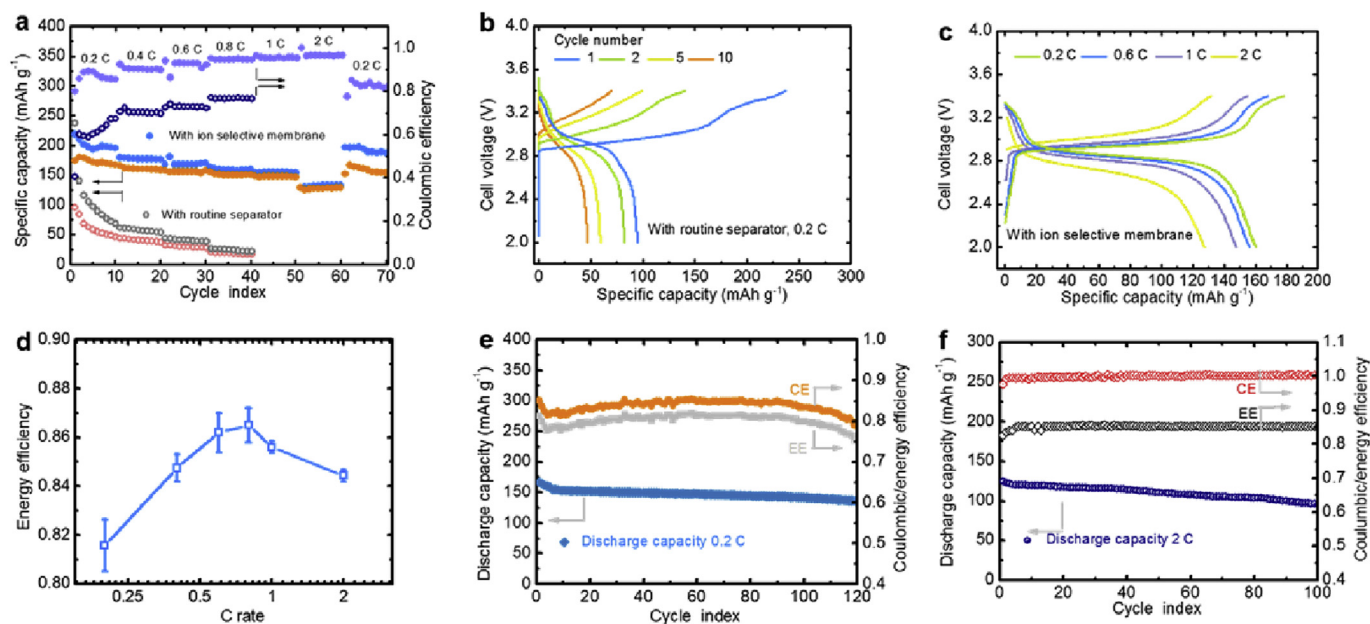


Fig. 4. (a) Comparison of rate performance of Li/PI batteries with a routine separator and a Nafion-functionalized composite membrane (Nafion loading 1.2 mg cm⁻²) using 1 M LiI₃ catholyte; (b) voltage profile of the Li/PI battery with a routine separator; (c) voltage profile of the Li/PI battery with a Nafion-functionalized composite membrane (ion selective Li/PI battery); (d) the effect of C rate on the ion selective Li/PI battery's energy efficiency; (e) cycling performance of the ion selective Li/PI battery at 0.2 C; (f) cycling performance of the ion selective Li/PI battery at 2 C. The C rate is calculated based on the specific capacity of elemental iodine (211 mAh g⁻¹).

(CE) increases at a higher current density. On the other hand, at a higher current density, the polarization will be increased, lowering the voltage efficiency (VE). As the energy efficiency is the product of coulombic and voltage efficiencies ($EE = CE \times VE$), an optimum in the energy efficiency will exist at a particular current density as shown in Fig. 4d.

To evaluate the long-term cycling performance, the Li/PI batteries were cycled at 0.2 C and 2 C respectively as shown in Fig. 4e and f. Stable cycling performances were achieved for both situations, suggesting that the batteries show excellent reversibility at higher rates and cycling stability at lower rates. Though the coulombic efficiency for 0.2 C cycling was relatively low (80%–85%), the discharge capacity did not undergo a visible drop. It is thereby speculated that the self-discharge behavior might occur in an electrochemical approach: $I_3^- + 2e^- \rightarrow 3I^-$, which induces minor change on the Li anode surface.

With these results, we compared the proposed Li/PI systems with Li-ion batteries and other Li based semi-liquid systems. It is found that iodine as an active material inherently shows its

advantage in terms of its gravimetric/volumetric energy density if compared with the existing cathode material such as LiCoO₂, LiMn₂O₄ and LiFePO₄ as can be seen in Fig. S7. On the other hand, in terms of the catholyte volumetric energy density, with the high solubility of active material, the Li/PI system is also more superior to the reported Li/polysulfide, Li/ferrocene and Li/TEMPO systems as can be found in Table S1 [15,43,44]. Also, with the Nafion-functionalized composite membrane the ion-selective Li/PI system demonstrates reasonably high coulombic and energy efficiencies. We also demonstrated that this type of Nafion-functionalized composite membrane was effective for other Li-halide semi-liquid battery systems [25,45]. When applied in a semi-liquid battery with polybromide as catholyte, stable cycling can be demonstrated as well (Figs. S8 and S9).

3.3. Electrochemical stability

Anode characterization was further exploited to examine whether the metallic lithium can be protected after long-term

cycling. Fig. 5(a–c) show the surface morphologies of the routine and cycled lithium anodes taken out of the batteries either with the routine separator or with the Nafion-functionalized composite membrane. In comparison to the fresh Li metal, for the one in the battery with a routine separator, the surface of the lithium anode becomes highly porous over cycling due to the corrosion of polyiodide shuttle. In sharp contrast, as shown in Fig. 5c, formation of lithium dendrite can be clearly observed for the battery protected by the Nafion-functionalized composite membrane after 50 cycles, in well consistency with the reported results [46]. As shown in the inset in Fig. 5c, after 120 cycles at 0.2 C, the dendrites become more protruding. The obtained results suggest that the lithium electro-deposition process has not been seriously affected by the corrosion of polyiodide shuttle and anode engineering tactics to address the lithium dendrite issue should be desirable for further research.

Electrochemical impedance spectroscopy results have further confirmed the above message. As presented in Fig. 5d, the semi-circle at the middle-frequency region (R_{SEI} and R_{ct}) is significantly enlarged after 5 cycles for the battery with the routine separator, which should be attributed to the increasingly non-uniform passivation layer. In contrast, only slight change of middle-frequency region is found for the case with the Nafion-functionalized composite membrane even after 120 cycles. Due to the high solubility of LiI and LiI_3 in ether-based solvents, there might not exist considerable active material loss during cycling. In this regard, we reason that one of the major attributes for capacity decay is the degradation of the lithium anode and the enlarged impedances [32,33,47–51].

In addition to the anode characterization, direct observation of the crossover phenomena helps to evaluate the stability of the battery system. As shown in Fig. 6a, we used a visible H-cell to simulate the charge process of the Li/PI battery. Specifically, we

focus on the charging process, as the infinite charging induced by the shuttle effect is a critical issue facing Li/PI battery. Blank electrolyte and 15 mL 25 mM LiI solution with a theoretical capacity of 10.0 mAh ($LiI \rightarrow I_2$) were added into the anode and cathode chambers respectively. The visible cell was charged with a rate of 1.2 mA, after every 1 h charge duration the battery was rested for 5 min to allow for the redistribution of polyiodide species. As can be seen in Fig. 6b, the cell voltage linearly climbed up over the charge process attaining a charge capacity of ~6.0 mAh, indicating that LiI in the cathode chamber has been mostly converted to LiI_3 . Meanwhile, during the charge process, polyiodide with a red-brown color was continuously generated around the carbon cloth electrode and the polyiodide concentration can be visibly found to increase. With the incorporation of Nafion-functionalized composite membrane, polyiodides could be well accommodated within the cathode side, only slight color change in the anode chamber could be observed for a duration of 5 h. Also, for a storage time of 8 h, there was no obvious color change in the anode side. In contrast, when we replaced the Nafion-functionalized composite membrane with the routine separator, it was found that the polyiodide crossover occurred in a very rapid manner, for the duration of less than 1 h, the polyiodide species had migrated from the cathode to the anode chamber, which was confirmed by the cell voltages during storage shown in Fig. 6c. Under the same storage time, induced by self-discharge, the battery with a routine separator showed a much faster cell voltage drop. Therefore, the achieved results clearly indicate that the membrane performs a substantial role to shield the Li anode from the polyiodide shuttle attack.

4. Conclusion

In summary, the Nafion-functionalized composite membrane

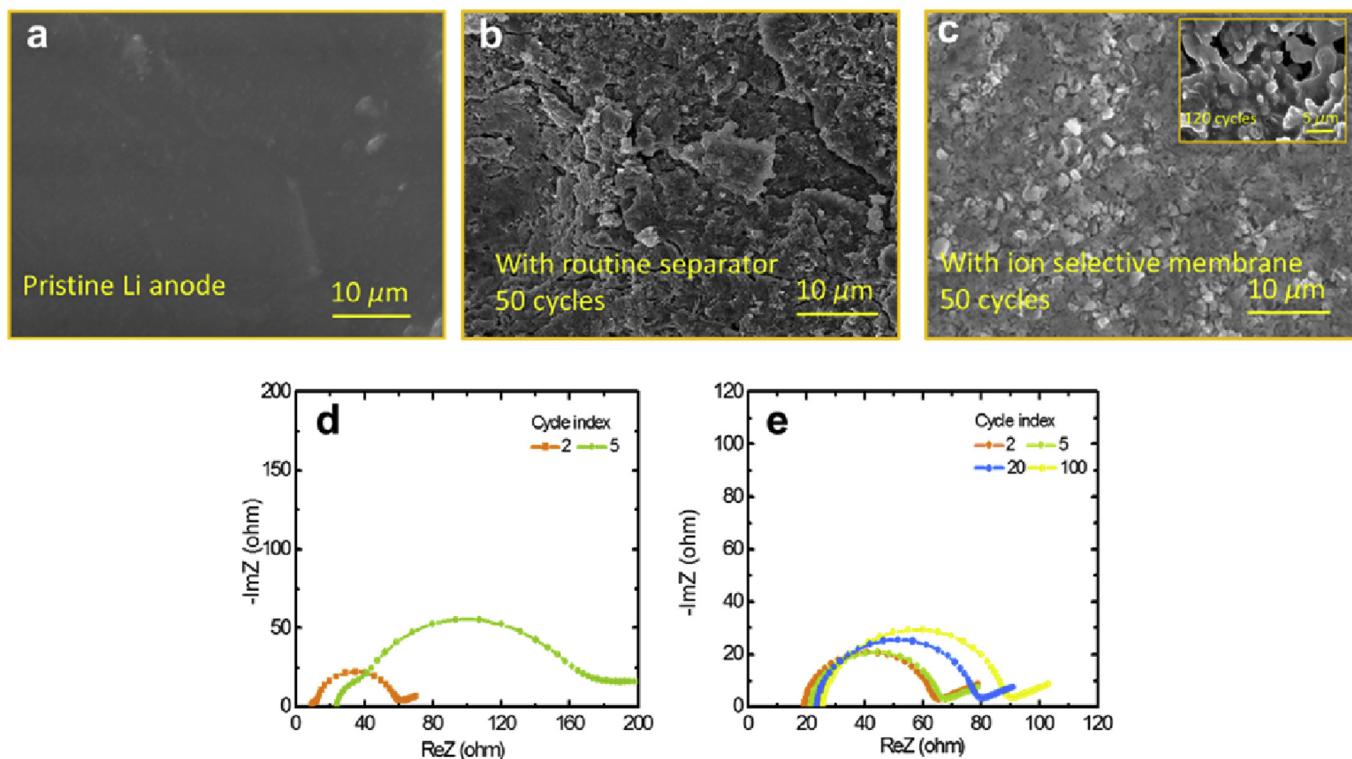


Fig. 5. (a) Pristine metallic lithium anode; (b) Li anode in the Li/PI battery with a routine separator after 50 cycles; (c) Li anode in the Li/PI battery with a Nafion-functionalized composite membrane (Nafion loading 1.2 mg cm^{-2}) after 50 cycles, the inset shows the Li anode after 120 cycles; (d, e) EIS results after charge: (d) the Li/PI battery with a routine separator; (e) the Li/PI battery with a Nafion-functionalized composite membrane.

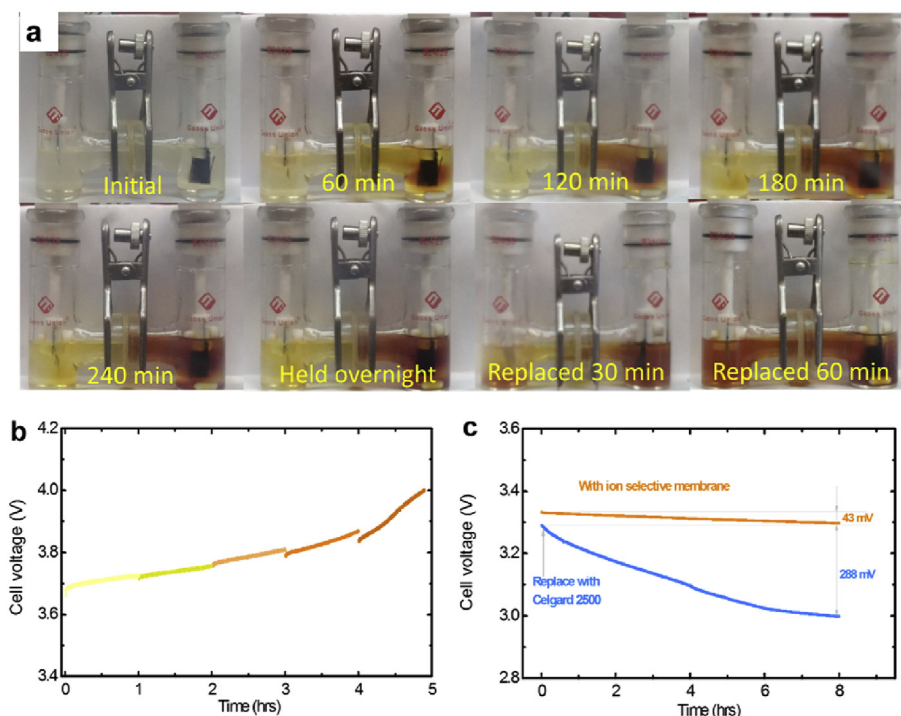


Fig. 6. (a) The optical images for the generation and diffusion of polyiodide during the charge process, initially a Nafion-functionalized composite membrane was exploited and the battery was charged for 5 h. After being held overnight, the electrolytes were extracted and the Nafion-functionalized composite membrane was replaced by a routine Celgard 2500 separator. (b) The charge profile for the transparent battery with the Nafion-functionalized composite membrane. (c) After charge, the transparent battery's resting voltage.

was exploited for semi-liquid Li/polyiodide batteries, which allowed the free transportation of lithium cations and suppression of polyiodide shuttle due to the electrostatic interactions. The resultant batteries showed a greatly improved cycling stability with a capacity decay of 0.16% per cycle for over 100 cycles, indicating that the use of the Nafion-functionalized composite membrane is highly effective in building a complete anion shield. With these results, we envisage that the shuttle effect could be overcome in the aprotic Li/polyiodide battery configuration, which offers promising opportunities for Li based flow battery research.

Acknowledgment

Y.X. Ren and M. Liu contributed equally to this work. The work was fully supported by Research Grants Council of the Hong Kong Special Administrative Region, China (Project No. 16213414).

Appendix A. Supplementary data

Supplementary data related to this article can be found at <http://dx.doi.org/10.1016/j.jpowsour.2016.12.043>.

References

- [1] Z. Yang, J. Zhang, M.C.W. Kintner-Meyer, X. Lu, D. Choi, J.P. Lemmon, J. Liu, *Chem. Rev.* 111 (2011) 3577–3613.
- [2] M. Armand, J.M. Tarascon, *Nature* 451 (2008) 652–657.
- [3] B. Dunn, H. Kamath, J.M. Tarascon, *Science* 334 (2011) 928–935.
- [4] M.S. Islam, C.A.J. Fisher, *Chem. Soc. Rev.* 43 (2014) 185–204.
- [5] J. Chen, F. Cheng, *Accounts Chem. Res.* 42 (2009) 713–723.
- [6] Y.X. Ren, T.S. Zhao, P. Tan, Z.H. Wei, X.L. Zhou, *Appl. Energy* 187 (2017) 706–716.
- [7] Y. Ren, T. Zhao, M. Liu, P. Tan, Y. Zeng, *J. Power Sources* 336 (2016) 115–125.
- [8] M. Liu, D. Zhou, Y.-B. He, Y. Fu, X. Qin, C. Miao, H. Du, B. Li, Q.-H. Yang, Z. Lin, *Nano Energy* 22 (2016) 278–289.
- [9] M. Liu, H. Jiang, Y. Ren, D. Zhou, F. Kang, T. Zhao, *Electrochim. Acta* 213 (2016) 871–878.
- [10] M. Liu, D. Zhou, H. Jiang, Y. Ren, F. Kang, T. Zhao, *Nano Energy* 28 (2016) 97–105.
- [11] P. Bai, J. Li, F.R. Brushett, M.Z. Bazant, *Energy Environ. Sci.* 9 (2016) 3221–3229.
- [12] H. Jiang, Z. Lu, M. Wu, F. Ciucci, T. Zhao, *Nano Energy* 23 (2016) 97–104.
- [13] Y. Yang, G. Zheng, Y. Cui, *Energy Environ. Sci.* 6 (2013) 1552–1558.
- [14] X. Wei, W. Xu, M. Vijayakumar, L. Cosimbescu, T. Liu, V. Sprenkle, W. Wang, *Adv. Mater.* 26 (2014) 7649–7653.
- [15] Y. Ding, Y. Zhao, G. Yu, *Nano Lett.* 15 (2015) 4108–4113.
- [16] P. Bai, M.Z. Bazant, *Nat. Commun.* 5 (2014).
- [17] Y. Lu, J.B. Goodenough, *J. Mater. Chem.* 21 (2011) 10113–10117.
- [18] Y. Lu, J.B. Goodenough, Y. Kim, *J. Am. Chem. Soc.* 133 (2011) 5756–5759.
- [19] Y. Zhao, M. Hong, N. Bonnet Mercier, G. Yu, H.C. Choi, H.R. Byon, *Nano Lett.* 14 (2014) 1085–1092.
- [20] Y. Zhao, Y. Ding, Y. Li, L. Peng, H.R. Byon, J.B. Goodenough, G. Yu, *Chem. Soc. Rev.* 44 (2015) 7968–7996.
- [21] Y. Zhao, H.R. Byon, *Adv. Energy Mater.* 3 (2013) 1630–1635.
- [22] Y. Zhao, L. Wang, H.R. Byon, *Nat. Commun.* 4 (2013).
- [23] Y. Zhao, Y. Ding, J. Song, L. Peng, J.B. Goodenough, G. Yu, *Energy Environ. Sci.* 7 (2014) 1990–1995.
- [24] H. Pan, X. Wei, W.A. Henderson, Y. Shao, J. Chen, P. Bhattacharya, J. Xiao, J. Liu, *Adv. Energy Mater.* 5 (2015).
- [25] P. Bai, M.Z. Bazant, *Electrochim. Acta* 202 (2016) 216–223.
- [26] H. Chen, Y.C. Lu, *Adv. Energy Mater.* 6 (2016).
- [27] Y.L. Wang, Q.L. Sun, Q.Q. Zhao, J.S. Cao, S.H. Ye, *Energy Environ. Sci.* 4 (2011) 3947–3950.
- [28] Q. Zhao, Y. Lu, Z. Zhu, Z. Tao, J. Chen, *Nano Lett.* 15 (2015) 5982–5987.
- [29] S. Evers, T. Yim, L.F. Nazar, *J. Phys. Chem. C* 116 (2012) 19653–19658.
- [30] S.S. Zhang, *Electrochim. Acta* 70 (2012) 344–348.
- [31] Z. Liang, G. Zheng, C. Liu, N. Liu, W. Li, K. Yan, H. Yao, P.-C. Hsu, S. Chu, Y. Cui, *Nano Lett.* 15 (2015) 2910–2916.
- [32] Z. Li, J. Huang, B.Y. Liaw, V. Metzler, J. Zhang, *J. Power Sources* 254 (2014) 168–182.
- [33] X.B. Cheng, R. Zhang, C.Z. Zhao, F. Wei, J.G. Zhang, Q. Zhang, *Adv. Science* (2015).
- [34] K.A. Mauritz, R.B. Moore, *Chem. Rev.* 104 (2004) 4535–4585.
- [35] H.Y. Liang, X.P. Qiu, S.C. Zhang, W.T. Zhu, L.Q. Chen, *J. Appl. Electrochem.* 34 (2004) 1211–1214.
- [36] Y. Lei, B. Zhang, B. Bai, T.S. Zhao, *J. Power Sources* 299 (2015) 202–211.
- [37] X.-G. Yang, Q. Ye, P. Cheng, T.S. Zhao, *Appl. Energy* 145 (2015) 306–319.
- [38] X. Yu, J. Joseph, A. Manthiram, *J. Mater. Chem. A* 3 (2015) 15683–15691.
- [39] Z. Cai, Y. Liu, S. Liu, L. Li, Y. Zhang, *Energy Environ. Sci.* 5 (2012) 5690–5693.
- [40] I. Bauer, S. Thieme, J. Brückner, H. Althues, S. Kaskel, *J. Power Sources* 251 (2014) 417–422.

- [41] Y. Zeng, T. Zhao, L. An, X. Zhou, L. Wei, J. Power Sources 300 (2015) 438–443.
- [42] Y.V. Mikhaylik, J.R. Akridge, J. Electrochem. Soc. 151 (2004) A1969–A1976.
- [43] X. Wei, W. Xu, M. Vijayakumar, L. Cosimbescu, T. Liu, V. Sprenkle, W. Wang, Adv. Mater. 26 (2014) 7649–7653.
- [44] Y. Yang, G. Zheng, Y. Cui, Energy Environ. Sci. 6 (2013) 1552–1558.
- [45] P. Bai, V. Viswanathan, M.Z. Bazant, J. Mater. Chem. A 3 (2015) 14165–14172.
- [46] W. Li, H. Yao, K. Yan, G. Zheng, Z. Liang, Y.-M. Chiang, Y. Cui, Nat. Commun. 6 (2015), 1274–1279.
- [47] D. Aurbach, E. Zinigrad, H. Teller, P. Dan, J. Electrochem. Soc. 147 (2000) 1274–1279.
- [48] W. Xu, J. Wang, F. Ding, X. Chen, E. Nasybulin, Y. Zhang, J.G. Zhang, Energy Environ. Sci. 7 (2014) 513–537.
- [49] H. Kim, G. Jeong, Y.U. Kim, J.H. Kim, C.M. Park, H.J. Sohn, Chem. Soc. Rev. 42 (2013) 9011–9034.
- [50] G. Zheng, S.W. Lee, Z. Liang, H.W. Lee, K. Yan, H. Yao, H. Wang, W. Li, S. Chu, Y. Cui, Nat. Nanotechnol. 9 (2014) 618–623.
- [51] X.B. Cheng, T.Z. Hou, R. Zhang, H.J. Peng, C.Z. Zhao, J.Q. Huang, Q. Zhang, Adv. Mater. 28 (2016) 2888–2895.